Current Optics and Photonics
Vol. 3, No. 5, October 2019, pp. 401-407

ISSN: 2508-7266(Print) / ISSN: 2508-7274(Online)
DOI: https://doi.org/10.3807/COPP.2019.3.5.401

# Polymer-waveguide Bragg-grating Devices Fabricated Using Phase-mask Lithography

**Tae-Hyun Park, Sung-Moon Kim, and Min-Cheol Oh***

*Department of Electronics Engineering, Pusan National University, Busan 46241, Korea*

(Received June 27, 2019 : revised August 5, 2019 : accepted August 8, 2019)

Polymeric optical waveguide devices with Bragg gratings have been investigated, for implementing tunable lasers and wavelength filters used in wavelength-division-multiplexed optical communication systems. Owing to the excellent thermo-optic effect of these polymers, wavelength tuning is possible over a wide range, which is difficult to achieve using other optical materials. In this study the phase-mask technology, which has advantages over the conventional interferometeric method, was introduced to facilitate the fabrication of Bragg gratings in polymeric optical waveguide devices. An optical setup capable of fabricating multiple Bragg gratings simultaneously on a 4-inch silicon wafer was constructed, using a 442-nm laser and phase mask. During fabrication, some of the diffracted light in the phase mask was totally reflected inside the mask, which affected the quality of the Bragg grating adversely, so experiments were conducted to solve this issue. To verify grating uniformity, two types of wavelength-filtering devices were fabricated using the phase-mask lithography, and their reflection and transmission spectra were measured. From the results, we confirmed that the phase-mask method provides good uniformity, and may be applied for mass production of polymer Bragg-grating waveguide devices.

*Keywords* : Integrated optics, Polymer waveguide devices, Bragg reflector, Phase mask
*OCIS codes* : (110.4235) Nanolithography; (130.5460) Polymer waveguides; (130.3120) Integrated optics devices; (130.7408) Wavelength filtering devices

## I. INTRODUCTION

Polymeric optical waveguides with Bragg gratings have been utilized for implementing tunable-wavelength lasers and wavelength-selective filters, which are key components of wavelength-division-multiplexed (WDM) optical communication systems [1-4]. In WDM, if wavelength-tunable lasers can be used instead of preparing multiple fixed-wavelength light source modules for each color, then operation at different wavelengths can be selected using the same device, which can reduce system maintenance and inventory costs. Tunable-wavelength filters are useful for extracting a desired wavelength, selectively, from the WDM signal; for this purpose, narrow bandwidths and wide tuning ranges are preferred, to increase the number of receiving channels [5]. As the range of the tunable wavelength expands, the number of available channels also increases, indicating that the communication system's capacity can be increased seamlessly [6].

Polymeric optical waveguides exhibit excellent thermal confinement and a strong thermo-optic (TO) effect, which can yield large refractive-index modulation [7]. This large index tunability facilitates the use of digital optical switches and variable optical attenuators based on mode evolution and higher-order mode excitation [8, 9]. Moreover, in polymeric waveguide devices, wide tuning of the Bragg-reflection wavelength is possible, in terms of a simple TO tuning electrode [10, 11].

Methods of fabricating Bragg gratings include e-beam direct writing, Lloyd's mirror interferometry, and the phase-mask method. E-beam direct writing can produce microstructures with narrow beam linewidths, but presents stitching errors and a relatively slow patterning speed [12]. The Lloyd's mirror interferometer is suitable for initial

*Corresponding author: mincheoloh@pusan.ac.kr, ORCID 0000-0002-0849-2121
Color versions of one or more of the figures in this paper are available online.

This is an Open Access article distributed under the terms of the Creative Commons Attribution Non-Commercial License (http://creativecommons.org/licenses/by-nc/4.0/) which permits unrestricted non-commercial use, distribution, and reproduction in any medium, provided the original work is properly cited.

Copyright © 2019 Current Optics and Photonics

experimental purposes, because the period of the Bragg grating is adjustable, depending on the angle of the mirror. However, the alignment of the optical system must be strictly maintained to produce Bragg gratings with desired periods [13]. The phase-mask method has a wide range of tolerance with respect to the incidence angle and wavelength of light, and is suitable for the large-scale fabrication of Bragg gratings [14].

In this work we have developed a method for phase-mask lithography, and use it to fabricate polymeric-waveguide wavelength filters. Previous experiments using a phase mask to fabricate polymeric-waveguide Bragg gratings were not successful, because of inaccurate configuration of the illumination source [15]. By using a 442-nm He-Cd laser for illuminating through the phase mask, we constructed an optical setup to produce multiple Bragg gratings on a 4-inch silicon wafer. During the experiment we observed internal diffractions from the phase mask, which deteriorated the quality of the interference pattern; these were subsequently avoided by using a shadow mask. Two types of wavelength-filtering devices were fabricated using the phase mask, and their transmission and reflection spectra were measured to verify the quality of the Bragg gratings produced using the phase mask.

## II. PHASE-MASK LITHOGRAPHY

Depending on the diffraction orders used to produce the interference pattern, two types of phase-mask lithography are available. In the case of surface-normal incidence, two diffracted lights produce the interference pattern, and the transmitted light should be suppressed by adjusting the depth of the grating pattern on the phase mask. The transmitted light can be suppressed to approximately 2% with a conventional phase mask [16]. In the other type of phase mask, light is incident at the Littrow angle and generates diffracted light and transmitted light, as shown in Fig. 1(a), to produce an interference fringe. The diffraction angle of the $m^{th}$ diffracted light, $\theta_m$, is given as follows:

$$m \cdot \frac{2\pi}{\Lambda_p} = \left(\sin\theta_i + \sin\theta_m\right) \cdot \frac{2\pi}{\lambda}, \tag{1}$$

where $\theta_i$ is the incident angle and $\Lambda_p$ is the period of the phase mask. Under the Littrow condition, the first-order diffraction angle becomes:

$$\theta_1 = \theta_i = \sin^{-1}\left(\frac{\lambda}{2\Lambda_p}\right). \tag{2}$$

The condition for suppressing second-order diffraction is obtained from Eq. (1), and another condition to support first-order diffraction can be found from Eq. (2), yielding the range of available wavelength of illuminating light:

$$\left(\frac{2}{3}\right) \cdot \Lambda_p \le \lambda \le 2 \cdot \Lambda_p. \tag{3}$$

The period of the phase mask used in this experiment was 540 nm, and the available wavelength range of incident light was from 360 to 1080 nm. Multiple Bragg-grating patterns with the phase mask could be produced in a single exposure step, over a wide area of substrate, as shown in Fig. 1(b).

A He-Cd laser with a wavelength of 442 nm was selected as the light source, considering the absorption spectrum of the photoresist. The optical setup for fabricating the Bragg grating over a wide area was constructed as shown in Fig. 2. The beam was filtered spatially, and expanded as it

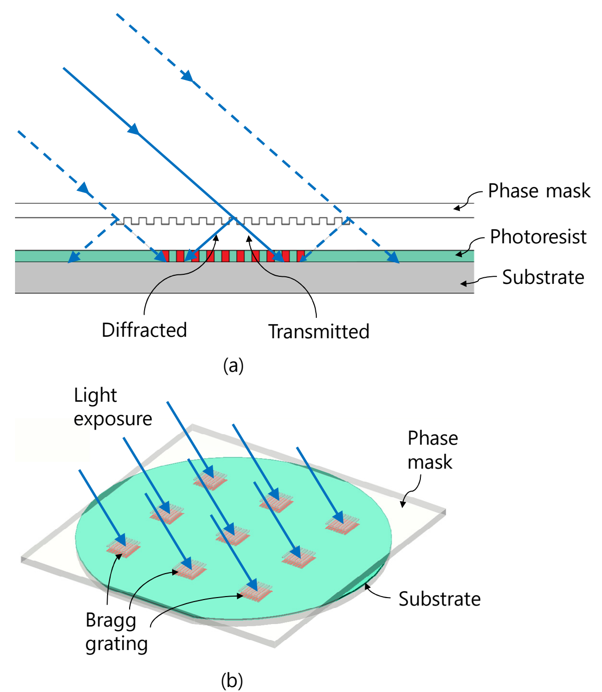


FIG. 1. Schematic diagram of (a) the two-beam interference pattern produced by the phase mask, and (b) Bragg-grating fabrication on a 4-inch wafer, using a phase mask with multiple patterns.

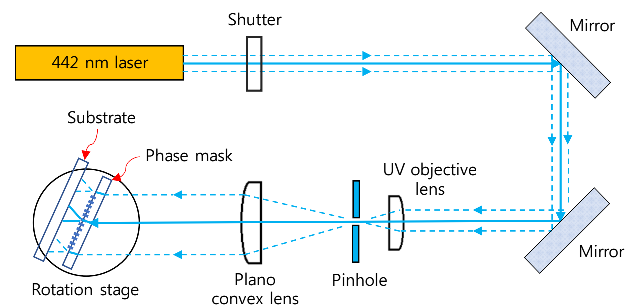


FIG. 2. Configuration of the phase-mask exposure setup, consisting of a spatial filtering setup and a collimating lens.

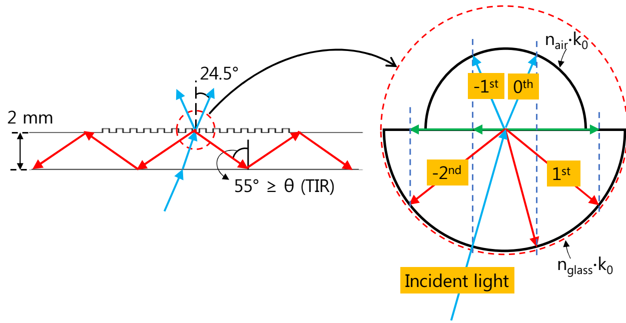


FIG. 3. *k*-vector diagram explaining the several diffraction orders produced by the phase mask. Additional diffraction orders are observed inside the substrate, which propagate via the phenomenon of total internal reflection.

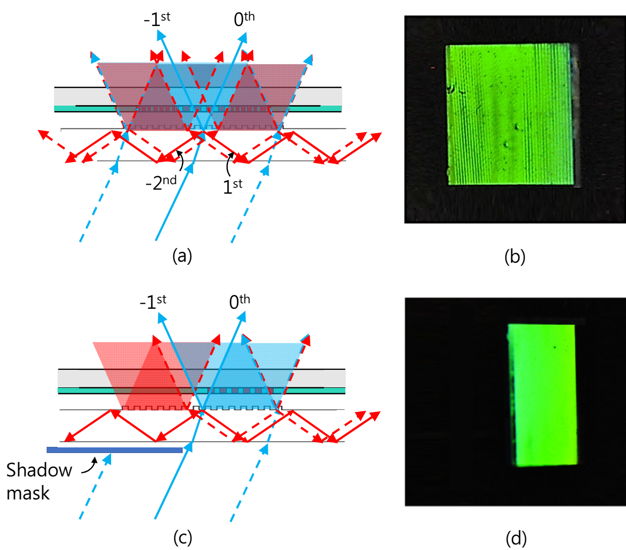


FIG. 4. (a) The arrows indicate four diffracted light beams from the center of the phase mask, and show the overlap of the incident and TIR light. (b) The produced grating has an undesirable long-period pattern, because of the contributions of the -2nd and 1st diffracted light beams inside the phase-masked substrate. (c) Using a shadow mask, overlap of light can be prevented by reducing the exposure area. (d) The bright, uniform grating pattern obtained using the shadow mask.

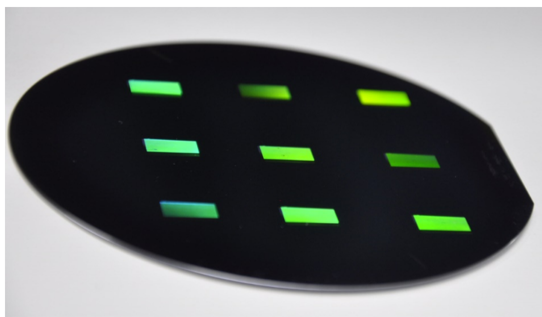

FIG. 5. Photograph of Bragg-grating patterns fabricated on a 4-inch wafer using the proposed method of phase-mask lithography.

passed through the pinhole and an objective lens. This expanded beam was collimated by a convex lens and irradiated onto the phase mask to produce first-order diffracted light and transmitted light. The two light beams interfered with each other to form an interference pattern with the same period as the phase mask. It was not necessary to maintain the gap between substrate and phase mask, because the interference pattern was established immediately after the light passed through the phase mask. However, to prevent contamination of the phase mask by contact with the photoresist, we inserted a thin spacer in between. The incident light's polarization was adjusted to *S*-pol with respect to the substrate, as determined in the phase-mask design, and the grating line became parallel to the polarization direction. However, in this process other higher-order diffractions could occur, especially into the glass substrate of the phase mask, as depicted in the *k*-vector diagram of Fig. 3.

For the 442-nm source light and phase-mask period of 540 nm, the angle of the diffracted light with respect to the surface normal was 24.5°, while the diffracted light inside the substrate had an angle of 55.0°, resulting in total internal reflection (TIR). Because the substrate had a thickness of 2 mm, the TIR light was shifted laterally by 5.7 mm, as shown in Fig. 4(a), and then mixed with the original incident light. As a result, the produced grating pattern exhibited a strange long-period pattern, as shown in Fig. 4(b). To avoid this problem, we subsequently used a shadow mask to reduce the exposed area (Fig. 4(c)), and then the TIR light was separated from the original incident light to produce a grating pattern of good quality, as in Fig. 4(d). Using the shadow mask, phase-mask lithography was performed several times in sequence, to produce multiple grating patterns over a wide area on a 4-inch substrate, as shown in Fig. 5.

## III. EXPERIMENT ON POLYMERIC-WAVEGUIDE BRAGG-GRATING DEVICES

Two types of polymeric-waveguide Bragg-grating devices, shown in Fig. 6, were fabricated to evaluate the quality of the Bragg gratings fabricated using a phase mask. A tunable-wavelength filter connected to a superluminescent laser diode (SLD) produced a tunable laser with an external cavity, as shown in Fig. 6(a). The tilted Bragg grating in Fig. 6(b) was useful to produce a wavelength filter capable of operating without external optical circulators. The detailed operating principle and design procedure can be found in our previous publications [17, 18].

The fabrication procedure for the proposed Bragg-grating filter is schematically shown in Fig. 7. The lower cladding layer of thickness 8 μm was formed by spin coating ZPU polymer (Chemoptics), with a refractive index of 1.430, on a 4-inch silicon wafer, which was then cured in a UV

chamber for five minutes. A diluted TSMR photoresist of thickness 150 nm was coated on the lower cladding layer, and then phase-mask lithography was performed on the entire wafer using the setup shown in Fig. 2. To characterize the sensitivity of the photoresist, we have tested various conditions. The initial laser power of 150 mW before the pinhole was expanded to produce an exposure power density of 0.87 mW/cm$^2$. Exposure time of 80-100 s was appropriate for producing a grating of good quality, with a period of 540 nm and forming 9259 elements over a length of 5 mm. It was transferred onto the lower cladding through oxygen-plasma etching to have a modulation depth of 200 nm, producing an effective index fluctuation of 0.0007 due to the grating. The core layer, with a refractive index of 1.455 and thickness of 2.8 μm, was formed on the lower cladding. The waveguide pattern of thickness 1.4 μm was fabricated using AZ 5214 photoresist. The straight waveguide pattern was aligned perpendicular to the Bragg grating, and another waveguide with an asymmetric Y-branch was aligned with the Bragg grating at an angle of 87.5°. The core layer was then etched by 2.2 μm to define a rib-type waveguide, as shown in the SEM image and microphotograph of Fig. 8. In this case, the effective index becomes 1.4429 for a waveguide width of 6 μm. The asymmetric Y-branch consisted of a two-mode waveguide of width 7 μm, a narrow waveguide of width 3 μm, and a wide waveguide of width 4 μm. Finally, the same polymer used for the lower cladding layer was used once again to form an upper cladding layer of thickness 8 μm.

The characterization setup was prepared as shown in Fig. 9. An SLD with center wavelength of 1550 nm and bandwidth of 100 nm was prepared. Through an isolator, polarization controller, and circulator, light was launched onto the straight-waveguide filter, and the reflected signal was observed using an optical spectrum analyzer (OSA). In the tilted Bragg-grating filter, the input light was launched onto the narrow waveguide, which was then evolved adiabatically into the odd mode when it arrived at the two-mode waveguide. Reflection by the tilted grating produced mode conversion between odd and even modes, which yielded the even mode, in this case. The reflected even mode evolved toward the wide waveguide through adiabatic mode conversion. These ideal mode-conversion procedures could be defined as a narrow-odd-even-wide (NOEW) process [19]. In addition, due to the crosstalk of

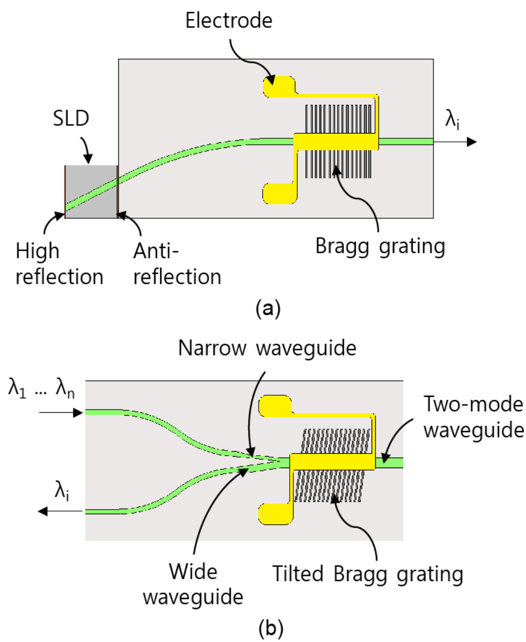


FIG. 6. Bragg-grating applications: (a) a tunable-wavelength laser and (b) a tunable-wavelength filter with separate output channel.

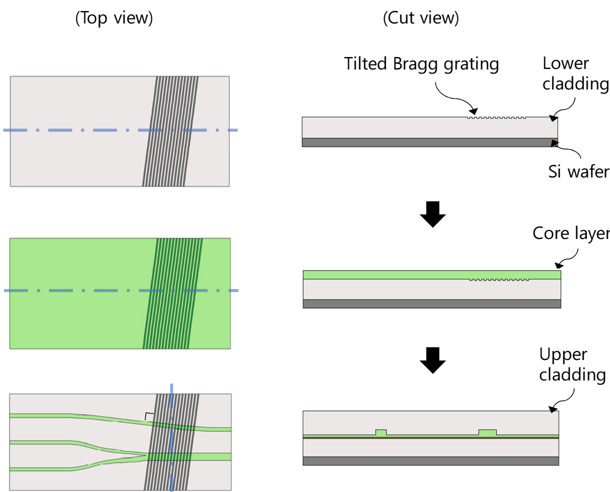


FIG. 7. Fabrication procedure of the polymeric-waveguide Bragg-grating filter (note that the cut-view angle is rotated in the third step of the figure).

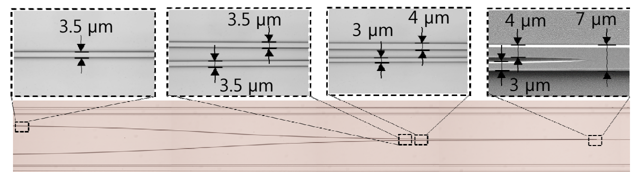


FIG. 8. Microphotograph of the asymmetric Y-branch waveguide, and a SEM image of the branch vertex.

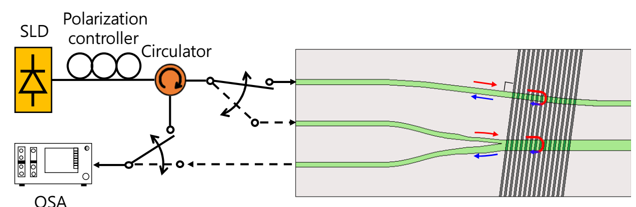


FIG. 9. Transmission and reflection measurement setup for a straight waveguide with a normal grating, and an asymmetric Y-branch waveguide with a tilted grating.

the asymmetric-Y branch, signals produced by narrow-even-odd-narrow (NEON) conversion or narrow-even-even-wide (NEEW) conversion could also be observed. If the tilted Bragg grating were unable to suppress the odd-odd coupling sufficiently, then the signal from narrow-odd-odd-narrow (NOON) conversion would also appear.

The reflection and transmission spectra of the straight-waveguide Bragg gratings with length 2 cm and widths 4, 6, and 8 μm were measured as shown in Fig. 10. For the width of 4 μm, the reflectance was 99.3% and the transmission dip was 21.8 dB with a center wavelength of 1556.7 nm. The bandwidths for 0.5 dB, 10 dB, and 20 dB were 0.55 nm, 1.17 nm, and 4.61 nm respectively. For the width of 6 μm, the reflectance was 99.9% and the transmission dip was 31.3 dB with a center wavelength of 1559.9 nm, which implied that a uniform Bragg grating was produced using the phase mask. The bandwidths for 0.5 dB, 10 dB, and 20 dB were 0.45 nm, 1.21 nm, and 3.75 nm respectively. For the width of 8 μm, the reflectance was 99.4% and the transmission dip was 22.7 dB with a center wavelength of 1561.0 nm. The insertion loss was 4.3 dB, which included a mode-mismatch loss of 1.6 dB/facet for single-mode fiber coupling and a propagation loss of 0.5 dB/cm. The difference in transmission-dip depth is caused by uneven end-facet conditions, because the end facet of the waveguide was simply diced, without careful polishing.

To evaluate the sensitivity of filter performance to tilt angle, we prepared a series of devices with varying width of the two-mode waveguide. Depending on the waveguide's width, the profile of the odd mode changed significantly, and the optimum tilt angle for preventing odd-odd mode coupling was affected. Hence, instead of fabricating devices with different tilt angles, we prepared devices with different two-mode-waveguide widths. The two-mode-waveguide width $W_t$ ranged from 6 to 14 μm, which corresponded to optimum tilt angles of 2.60° to 1.77°. The output wavelength spectra of the devices are shown in Fig. 11. For $W_t$ of 6 μm and 10 μm, the main NOEW peak appeared at 1555.4 nm and 1559.1 nm, as shown in Figs. 11(a) and 11(b) respectively. The peak arising from even-even mode coupling was observed at the longer wavelength because the asymmetric Y-branch had some crosstalk, which could be reduced by improving the Y-branch pattern resolution, by using a metal mask [20]. The peak at the shorter wave-

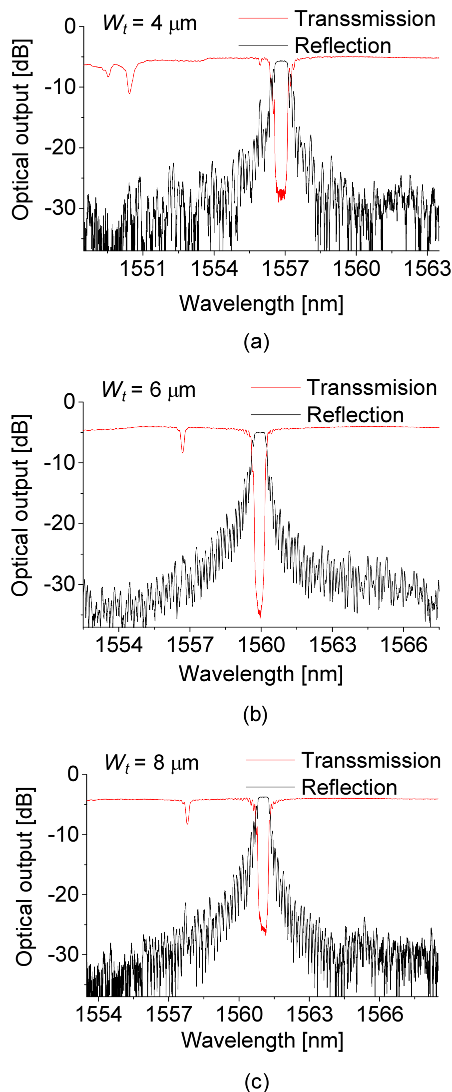


FIG. 10. Reflection and transmission spectra of straight-waveguide filters with various waveguide widths.

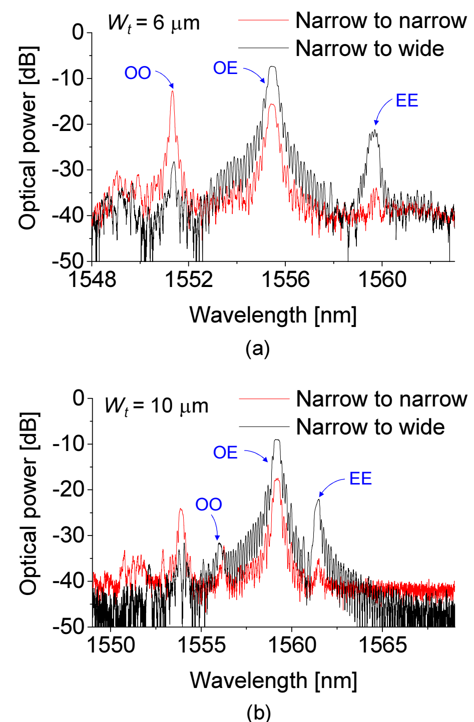


FIG. 11. Reflection and transmission spectra of asymmetric Y-branch waveguide filters with two-mode-waveguide widths of 6 and 10 μm.

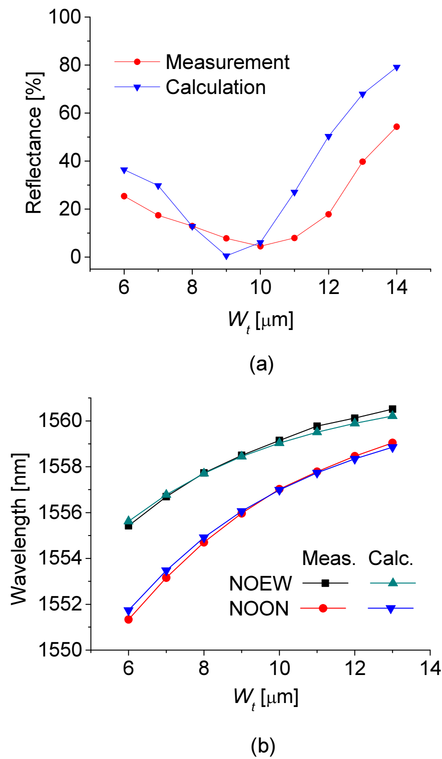


FIG. 12. (a) Odd-odd mode-coupling efficiency, shown by the reflectivity of NOON mode conversion, which corresponds well to the designed values, and (b) Bragg-reflection-peak wavelengths for odd-odd and odd-even coupling, depending on the two-mode-waveguide width.

length was caused by odd-odd coupling in the tilted grating.

For the devices of various $W_t$, the magnitudes of the NOON peaks were measured and compared to the designed values, as shown Fig. 12(a). The experimental results exhibited minimum odd-odd coupling at 10 μm, corresponding to a tilt angle of 2.24°, which was close to the designed value. The slight difference was caused by the patterning-width reduction during the dry-etching process.

The reflection-peak wavelengths are summarized in Fig. 12(b), to establish whether the effective mode indices of the two-mode waveguide were produced as designed. As t$W_t$ increased, the effective indices of the even and odd modes also increased, and the reflection shifted to longer wavelengths. The experimental results correspond well to the designed values, which confirms that the waveguide has the expected effective indices.

## IV. CONCLUSION

In this work we have introduced a phase-mask technology superior for mass production, when compared to existing interferometric systems. We used the proposed method to fabricate polymeric optical-waveguide Bragg gratings, and confirmed their characteristics. Grating uniformity deteriorated due to diffraction inside the substrate, so a shadow mask was used to prevent complicated interference. The phase-mask interference pattern was exposed sequentially to produce multiple Bragg-grating patterns over a wide range on a 4-inch silicon wafer. To evaluate the Bragg-grating pattern, we fabricated wavelength filters and measured their reflection and transmission spectra. In the straight-waveguide wavelength filter, the reflectance was more than 99% and the bandwidths for 0.5 dB, 10 dB, and 20 dB were 0.48 nm, 1.30 nm, and 4.25 nm respectively. A flat-top passband for WDM optical communication was achieved. In the tilted Bragg-grating filters, high reflectivity was observed and the reflection peaks corresponded well to the designed values. Prior to the practical use of this phase-mask technology for mass production of polymer-waveguide grating devices, the diffraction orders inside the substrate should be eliminated by considering the various diffraction orders and carefully selecting the wavelength of the illumination laser. For the manufacture of large-area gratings, a laser of sufficiently high power and a large collimation lens are needed.

## ACKNOWLEDGMENT

This work was supported by the National Research Foundation of Korea (NRF) grant funded by the Korea government (2017R1A2A1A17069702). The authors would like to thank Dr. Christian Buchwald of Ibsen Photonics for helpful discussion.

## REFERENCES


1. S.-H. Oh, K.-H. Yoon, K.-S. Kim, J. Kim, O.-K. Kwon, D.-K. Oh, Y.-O. Noh, J.-K. Seo, and H.-J. Lee, “Tunable external cavity laser by hybrid integration of a superluminescent diode and a polymer Bragg reflector,” IEEE J. Sel. Topics Quantum Electron. **17**, 1534-1541 (2011).
2. D. Felipe, Z. Zhang, W. Brinker, M. Kleinert, A. Maese-Novo, C. Zawadzki, M. Moehrle, and N. Keil, “Polymer-based external cavity lasers: Tuning efficiency, reliability and polarization diversity,” IEEE Photon. Technol. Lett. **26**, 1391-1394 (2014).
3. J.-H. Lee, M.-Y. Park, C.-Y. Kim, S.-H. Cho, W. Lee, G. Jeong, and B.-W. Kim, “tunable external cavity laser based on polymer waveguide platform for WDM access network,” IEEE Photon. Technol. Lett. **17**, 1956-1958 (2005).
4. L. Eldada, R. Blomquist, M. Maxfield, D. Pant, G. Boudoughian, C. Poga, and R. A. Norwood, “Thermooptic planar polymer Bragg grating OADM’s with broad tuning range,” IEEE Photon. Technol. Lett. **11**, 448-450 (1999).
5. D. Sadot and E. Boimovich, “Tunable optical filters for dense WDM networks,” IEEE Commun. Mag. **36**, 50-55 (1998).
6. J. Buus and E. J. Murphy, “Tunable lasers in optical networks,” J. Lightwave Technol. **24**, 5-11 (2006).

7. Y. Hida, H. Onose, and S. Imamura, "Polymer waveguide thermooptic switch with low electric power consumption at 1.3 μm," IEEE Photon. Technol. Lett. **5**, 782-784 (1993).
8. N. Keil, H. H. Yao, and C. Zawadzki, "2 × 2 digital optical switch realized by low cost polymer waveguide technology," Electron. Lett. **32**, 1470-1471 (1996).
9. Y.-O. Noh, C.-H. Lee, J.-M. Kim, W.-Y. Hwang, Y.-H. Won, H.-J. Lee, S.-G. Han, and M.-C. Oh, "Polymer waveguide variable optical attenuator and its reliability," Opt. Commun. **242**, 533-540 (2004).
10. T.-H. Park, S.-M. Kim, S.-H. Park, J.-K. Seo, H.-G. Lee, and M.-C. Oh, "Polymer waveguide WDM channel selector operating over the entire C and L bands," Opt. Express **26**, 16323-16332 (2018).
11. Z. Zhang, D. de Felipe, W. Brinker, M. Kleinert, A. Maese-Novo, M. Moehrle, C. Zawadzki, and N. Keil, "C/L-band colorless ONU based on polymer bi-directional optical subassembly," J. Lightwave Technol. **33**, 1230-1234 (2015).
12. C. Vieu, F. Carcenac, A. Pepin, Y. Chen, M. Mejias, A. Lebib, L. Manin-Ferlazzo, L. Couraud, and H. Launois, "Electron beam lithography: resolution limits and applications," Appl. Surf. Sci. **164**, 111-117 (2000).
13. Q. Xie, M. H. Hong, H. L. Tan, G. X. Chen, L. P. Shi, and T. C. Chong, "Fabrication of nanostructures with laser interference lithography," J. Alloys Compd. **449**, 261-264 (2008).
14. E. Gamet, Y. Jourlin, S. Pelissier, R. Min, S. Reynaud, C. Veillas, J. C. Pommier, and O. Parriaux, "Flying phase mask for the printing of long submicron-period stitching less gratings," Microelectron. Eng. **83**, 734-737 (2006).
15. M.-C. Oh, H.-J. Lee, M.-H. Lee, J.-H. Ahn, S.-G. Han, and H.-G. Kim, "Tunable wavelength filters with Bragg gratings in polymer waveguides," Appl. Phys. Lett. **73**, 2543-2545 (1998).
16. K. Buchwald, *Fused Silica Transmission Gratings*, Ibsen Photonics Corp., Farum, Denmark (2007).
17. Y.-O. Noh, H.-J. Lee, J. J. Ju, M.-S. Kim, S. H. Oh, and M.-C. Oh, "Continuously tunable compact lasers based on thermo-optic polymer waveguides with Bragg gratings," Opt. Express **16**, 18194-18201 (2008).
18. S.-H. Park, J.-K. Seo, J.-O. Park, H.-K. Lee, J.-S. Shin, and M.-C. Oh, "Transmission type tunable wavelength filters based on polymer waveguide Bragg reflectors," Opt. Commun. **362**, 96-100 (2016).
19. T.-H. Park, G. Huang, E.-T. Kim, and M.-C. Oh, "Optimization of tilted Bragg grating tunable filters based on polymeric optical waveguides," Curr. Opt. Photon. **1**, 214-220 (2017).
20. T.-H. Park, J.-S. Shin, G. Huang, W.-S. Chu, and M.-C. Oh, "Tunable channel drop filters consisting of a tilted Bragg grating and a mode sorting polymer waveguide," Opt. Express **24**, 5709-5714 (2016).